Static Aeroelastic Response of Chiral-core Airfoils

A. Spadoni and M. Ruzzene

Journal of Intelligent Material Systems and Structures 2007; 18; 1067 originally published online May 24, 2007;
DOI: 10.1177/1045389X06072361

Static Aeroelastic Response of Chiral-core Airfoils*

A. Spadoni and M. Ruzzene†

School of Aerospace Engineering, Georgia Institute of Technology, Atlanta, GA 30332, USA

ABSTRACT: Extensive research is being devoted to the analysis and application of cellular solids for the design of innovative structural components. The chiral geometry in particular features a unique mechanical behavior which is here exploited for the design of 2D airfoils with morphing capabilities. A coupled-physics model, comprising computational fluid dynamics and structural analyses, investigates the influence of the chiral core on the aerodynamic behavior of the airfoil. Specifically, the model predicts the static deflection of the airfoil as a result of given flow conditions. The morphing capabilities of the airfoil, here quantified as camber changes, are evaluated for various design configurations of the core.

Key Words: chiral geometry, truss-core airfoil, passive morphing.

INTRODUCTION

In recent years, several researchers have investigated structural concepts with morphing capabilities. The introduction of smart structures and adaptive technologies in the aerospace field offers exciting opportunities to implement previously inaccessible structural morphing concepts (McGowan et al., 2003). According to (Bowman et al., 2002), morphing in the engineering sense can be generally defined as 'a set of technologies that increases a vehicle's performance by manipulating certain characteristics to better match the vehicle state to the environment and task at hand'. Particularly to the aerospace field, the typical objective of a morphing concept is to provide airfoils with continuous deformations, and to eliminate the need for flap-type mechanisms. In this sense, a variety of solutions have recently been proposed to provide aircraft wings and helicopter rotor blades with adaptive capabilities. Methods to generate both chord-wise and span-wise camber variations are particularly investigated, with the goal of controlling aeroelastic and structural performance of wings and blades in response to changing flight conditions. The belt rib concept, for example, is an interesting solution proposed by Campanile and Sachau (2000). Continuous camber variation is achieved by transferring the stroke of an actuator into a geometric change of the airfoil shape through a closed belt and an internal network structure. A similar, remarkable solution for camber variation is the finger concept presented by (Monner et al., 1999), where the airfoil features a flexible rib composed of plate-like elements connected through revolute joints. The rotation of the driven element is transferred gradually from element to element thus providing the desired deformed profile. Tension–torsion coupling has been employed as an effective means to actively control camber variations in helicopter blades (Buter et al., 2000). Recent design solutions have considered inflatable airfoil structures (Cadogan et al., 2004), variable-span morphing wings (Bae et al., 2004; Trenker, 2003), and hingeless flexible leading and trailing edges actuated using shape memory alloys (Kudva, 2004).

In this article, a structural assembly that allows continuous conformability while maintaining load-carrying capabilities is proposed as an alternative design for airfoil morphing. The airfoil features a truss-core configuration with chiral topology of the kind investigated by (Spadoni et al., 2005). The static deformations of the airfoil due to air loads are evaluated through a coupled computational fluid dynamics (CFD)/structural analysis. The developed model is used to investigate the effects of the core design on the structural compliance of the airfoil.

The article is organized in five sections, including 'Introduction'. The section on 'concept' describes the considered configuration and its main geometric parameters, while the section on 'Numerical model of a chiral airfoil' presents the structural and CFD models and the iterative procedure devised to account for their interaction. The section on 'Compliance of chiral-core airfoils' presents the static aeroelastic

*Presented at the 16th International Conference on Adaptive Structures and Technologies (ICAST), October 9–12, 2005, Paris, France.

†Author to whom correspondence should be addressed.
E-mail: massimo.ruzzene@ae.gatech.edu

Figures 1, 3–9 and 11–18 appear in color online: http://jim.sagepub.com

1045-389X/07/10 1067–9 $10.00/0 DOI: 10.1177/1045389X06072361

performance of the considered airfoil designs. The concluding section summarizes the main results of the work and provides recommendation for future investigations.

CONCEPT

The proposed configuration features a truss-type structure hosted within the airfoil to generate a truss-core configuration (Figure 1). The core is arranged according to a chiral topology of the kind described in (Prall and Lakes, 1996), and shown in Figure 2. This topology is obtained through the assembly of circular elements acting as nodes, connected by ribs or ligaments tangent to the nodes. The resulting cellular structure is characterized by unique, non-classical mechanical properties. Previous work has shown the equivalent in-plane Poisson's ratio to be approximately -0.91. The negative Poisson's ratio behavior leads to unique deformation patterns, and corresponds to a very high in-plane shear modulus. In addition, the chiral structure is capable of undergoing large displacements while operating in the elastic range of the constitutive material. Moreover, the properties and the behavior of chiral assemblies can be significantly altered through variations in the characteristic parameters that define the geometry (R, L, β, and θ in Figure 2). This allows tailoring the properties of the assembly to achieve desired characteristics by changing a limited number of geometric parameters. The application of the chiral geometry for airfoil morphing has already been investigated in (Bornengo et al., 2005), where the performance of a conformable race car wing is investigated through a numerical model. Bornengo et al. (2005) considers the airfoil core as a homogeneous material with the mechanical properties of a homogenized chiral assembly. The results presented in Bornengo et al. (2005) provide the motivation for the current work, where a macroscopic chiral configuration is instead considered to investigate local as well as global deformations. Such a detailed model is considered in an effort to demonstrate large trailing-edge displacements within the linear elastic region of the constitutive material. The dynamic properties of an airfoil with chiral truss-core have previously been investigated in (Spadoni et al., 2005), where it is shown how the core is capable of generating localized dynamic deformations, which could be useful for active flow control. In this study, however, focus is placed on the static compliant characteristics of the structure. The airfoil deflects as a result of air loads evaluated through a weakly coupled sequential fluid-structural model. The compliant characteristics of the proposed design suggest its application for drag reduction, or as part of actively controlled airfoil configurations.

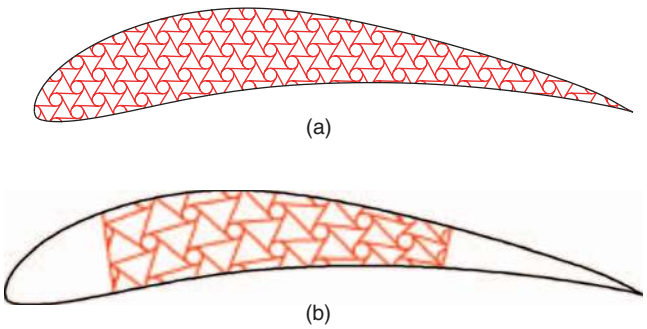

Figure 1. *Investigated configurations.*

NUMERICAL MODEL OF A CHIRAL AIRFOIL

The performance of the considered airfoil is investigated through weakly coupled structural and CFD models. The weak coupling is justified by the limited requirement of evaluating the deformed configuration of the airfoil resulting from steady aerodynamic loads defined by specified flow conditions. Within such an assumption, the structural displacements can be predicted through an iterative process where air loads and corresponding displacements are successively passed to the structural and fluid codes respectively to obtain convergence.

Structural Model

The static equilibrium state of the proposed airfoil configuration is predicted by a 2D finite element (FE) model, whereby beam and plane elements are used to discretize the structural system. In particular, the model shown in Figure 1a is analyzed using beam elements only, while the model shown in Figure 1b requires the use of both beam and planar elements, as part of the

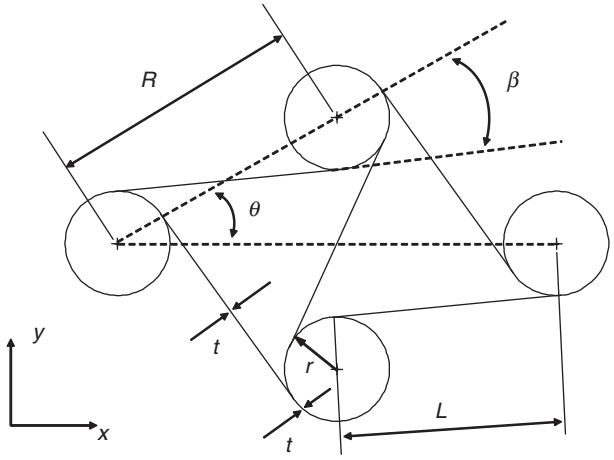

Figure 2. *Unit cell of a chiral configuration and characteristic parameters.*

leading and trailing edge regions are composed of a continuum material. The airfoil profile and chiral core are hence analyzed as a frame structure, with beam elements featuring both axial and transverse degrees of freedom (DOF). Transverse shear deformations are also included according to the formulation presented in (Cook et al., 2001), in order to avoid inaccuracies derived from the presence of non-slender elements. Classical isoparametric planar elements are employed to model the leading and trailing edge regions, where it is assumed that a homogeneous material is utilized. The mesh employed for such regions includes both triangular and quadrilateral elements of the kind shown in Figure 3. The quadrilateral elements are of the bilinear kind, developed according to the formulation denoted as *Q*6 in (Cook et al., 2001), while the planar triangular elements are constant strain elements. Both triangular and quadrilateral elements feature 'drilling' DOF's, which allow their coupling with the beam elements used for the chiral core and skin discretization.

Computational Fluid Dynamics Model

As relatively large deformations of the airfoil are to be investigated, no assumption regarding the linearity of the flow field, or resulting aerodynamic loads, is made. Rather, the entire flow field is resolved using the finite-volume Galerkin program NSC2KE (Mohammadi, 1994). The fluid region is discretized with the unstructured triangular mesh depicted in Figure 4. While the program NSC2KE offers a variety of viscous flow and boundary layer models, their use is beyond the scope of the current work, which aims at investigating static aeroelastic deformations caused by lift as opposed to drag. Nonetheless, the entire flow field is analyzed, albeit using an inviscid flow or Euler model (Mohammadi, 1994). In particular, the inflow and outflow boundaries (Figure 4a) are treated by a characteristic technique (Mohammadi, 1994), while on the airfoil profile, adiabatic wall or Newmann boundary conditions are used in conjunction with symmetry or slip conditions. The mesh of the elements in contact with the airfoil profile is selected in order to maintain maximum element side length at the trailing and leading edges equal to $1\times10^{-3}\times c$, with c denoting the airfoil chord. The element size over the rest of the airfoil profile, away from trailing and leading edges, is linearly relaxed by a factor of 5 (Figure 4b), since particularly unfavorable pressure gradients are not expected. This assumption produces triangular elements over the airfoil with a maximum side length varying between $10^{-3}\times c$, at the trailing and leading edges, to $5\times10^{-3}\times c$ at the mid curvilinear length, along the top and bottom portions of the airfoil. The relaxation of element size in the direction normal to the airfoil is not directly controlled. The inflow and outflow boundaries are discretized with 30 elements whose maximum side length, and the element size is reduced linearly as the airfoil is approached. The wake region is also discretized with the same logic as the airfoil boundaries: wake elements near the trailing edge of the wing profile share the same size imposed to elements on the airfoil boundary. Wake element size is then increased linearly up to the outflow boundary (Figure 4a). External forces such as gravitational forces are neglected as the inertial frame of reference is assumed to be at rest. An Euler local time stepping procedure is employed as the sought solution is assumed to be steady-state. The number of iterations required to resolve the flow field has been selected based on the considered mesh (Figure 4). In particular, both the residual's norm and the lift coefficient have been analyzed for a varying number of iterations. Figure 5a

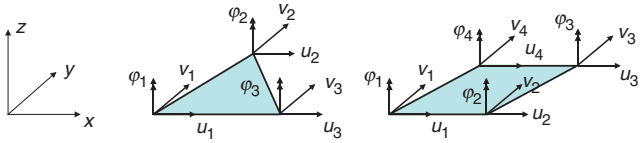

Figure 3. *Isoparametric planar elements.*

(a)

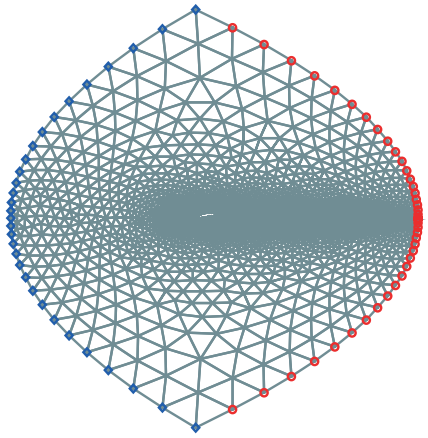

◇ Inflow points; o Outflow points

(b)

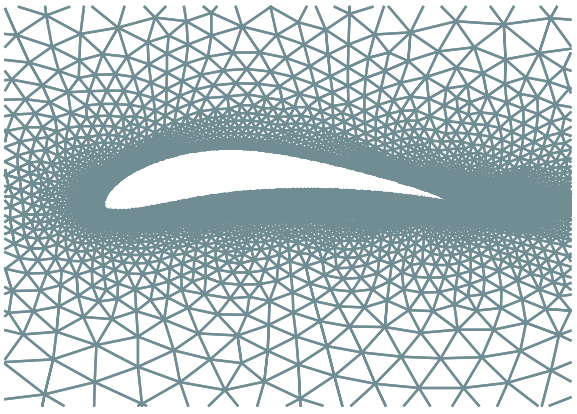

Detailed view of airfoil boundary

Figure 4. *CFD unstructured mesh.*

suggests that reasonable results can be obtained with ~4000–5000 iterations. Figure 5b, on the other hand, suggests that the normalized L_2 norm is reduced by four orders of magnitude with 8000 iterations. The latter number is then used as the current static aeroelastic investigation and requires the pressure distribution around the airfoil to then evaluate structural deformations, as opposed to investigating the global lift coefficient only.

Fluid-structure Interaction and Convergence

Coupled-field analyses may be carried out according to the sequential and direct methods. In the case of the direct method a coupled-field element type containing all necessary DOF is used. In the case of the sequential method, solutions for the fluid and solid analyses are carried out separately. Given the need for analyzing relatively large structural deformations, and thus potentially substantial changes in the flow field, a sequential method is used, whereby the static aeroelastic solution is obtained through an iterative process based on convergence of fluid and structural solutions. The computed gauge pressure at the fluid-airfoil boundary is applied as a distributed load on the structural model. Equilibrium is then imposed, and the resulting deformed configuration is used to obtain a newly meshed fluid region. The process is repeated until $L_i - L_{i-1} < 1 \times 10^{-3}$, with $L = \underline{u}^T \underline{u}$, where $\underline{u}$ is the vector of structural nodal DOFs, and i is the iteration number. The flow chart depicting the iterative procedure considered for the sequential method is shown in Figure 6. Typically, convergence is achieved after three or four iterations. An example of the obtained pressure distribution, having reached convergence, in the flow field is shown in Figure 7, while the associated pressure coefficient (C_P) over the airfoil boundary is depicted in Figure 8. No particular corrugations over the upper portion of the airfoil profile are observed. Such corrugations would be produced by pressure fluctuations over the profile, which would manifest themselves as discontinuities in the (C_P) distribution.

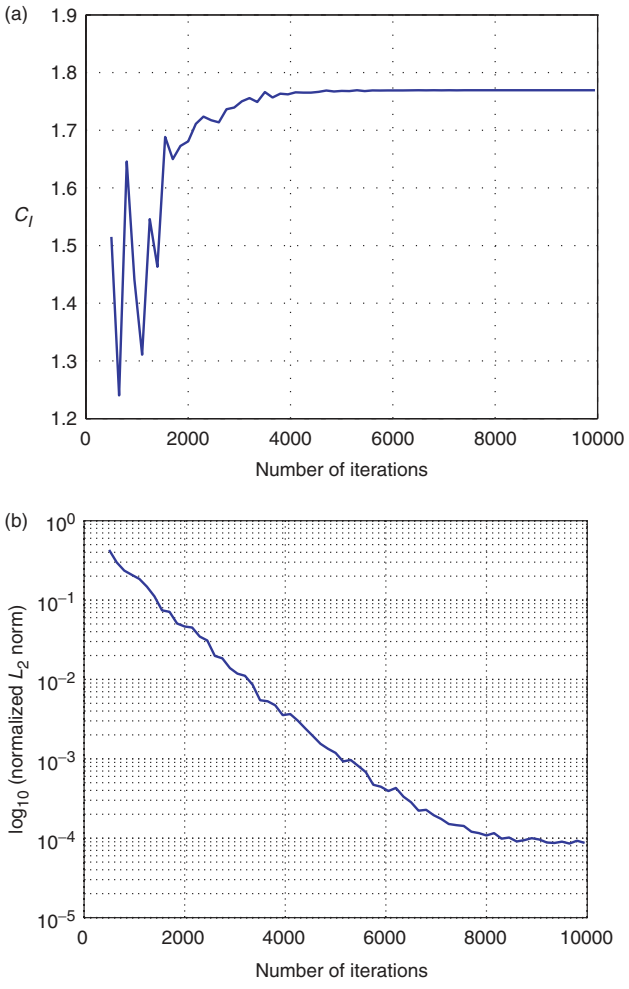

Figure 5. *Result convergence in terms of C_l (a), and L_2 norm (b).*

COMPLIANCE OF CHIRAL-CORE AIRFOILS

The considered airfoil section is an Eppler 420 profile. Such highly cambered airfoil is chosen to demonstrate the core compliance of the proposed assembly. The chosen truss-core airfoil configuration constitutes a system which theoretically presents high lift at low free-stream velocity, responsible for camber deformations; as the free-stream velocity is increased on the other hand, the system would reach a structurally stable low-camber, low-drag configuration. Structural stability, or a finite de-cambering event, is guaranteed by a faster growth of elastic loads than their aerodynamic counterparts. Aerodynamic loads produced by the proposed truss-core airfoil, in fact, tend to increase linearly with flow velocity, as opposed to the usual parabolic relationship.

Design Configuration 1

Initial investigations are carried out on the configuration shown in Figure 1a. The design is obtained by fitting a regular, periodic chiral layout into the airfoil shape. The regular chiral layout considered is shown in Figure 9a, with the superimposed Eppler 420 airfoil, of chord $c = 1$ m. Figure 9b shows the resulting truss-core airfoil. In the model, the leading edge is considered clamped. The out-of-plane depth of the assembly is 2.54 cm. The core is aluminum (Young's modulus $E = 7.1 \times 10^{10}$ N/m^2, density $\rho = 2700$ kg/m^3, Poisson's ratio $\nu = 0.33$) with a wall thickness $t = 0.8$ mm, while the outer skin is modeled as a softer material (Young's modulus $E = 9 \times 10^9$ N/m^2, density $\rho = 2700$ kg/m^3, Poisson's ratio $\nu = 0.33$) with a wall

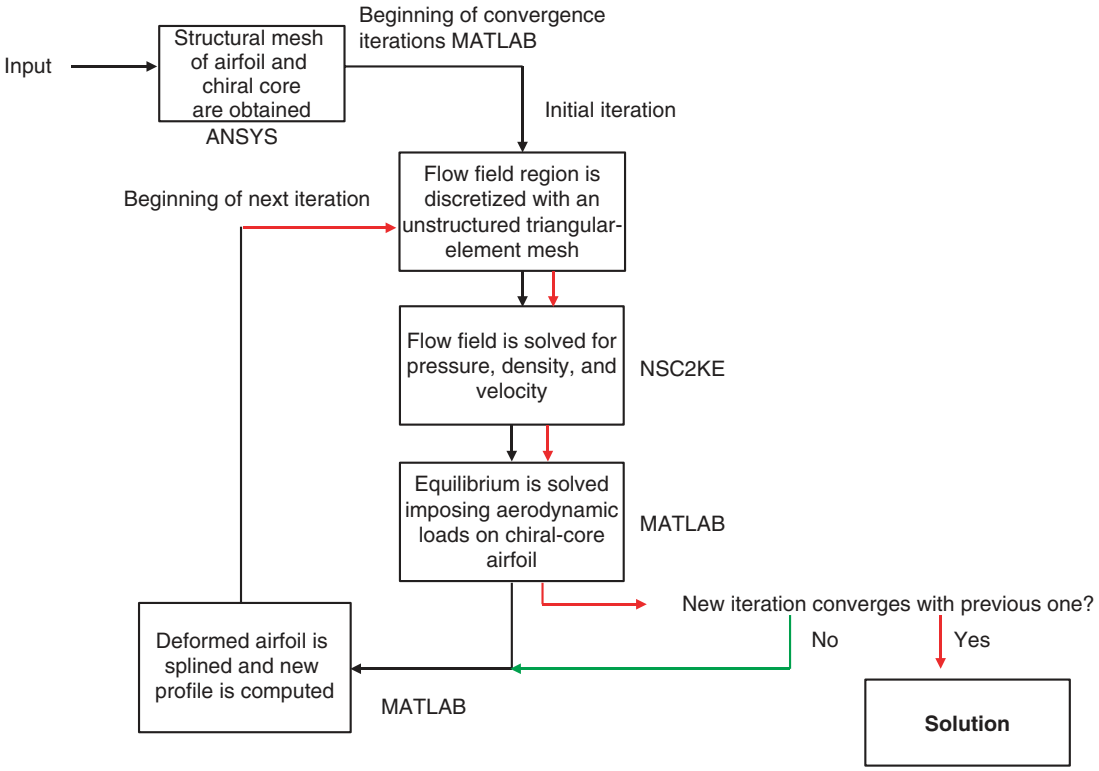

Figure 6. *Flow chart of fluid-structure iterative procedure.*

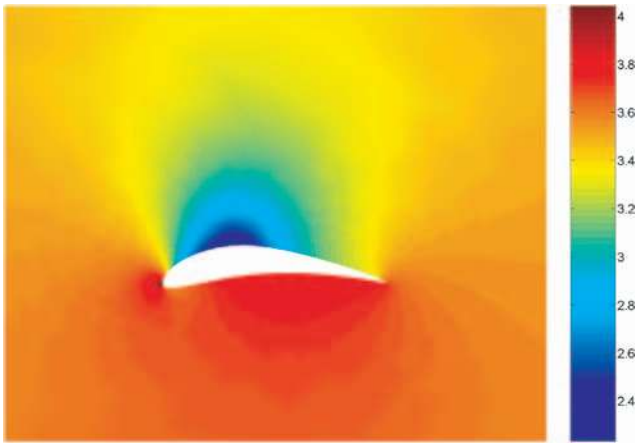

Figure 7. *Computed normalized pressure.*

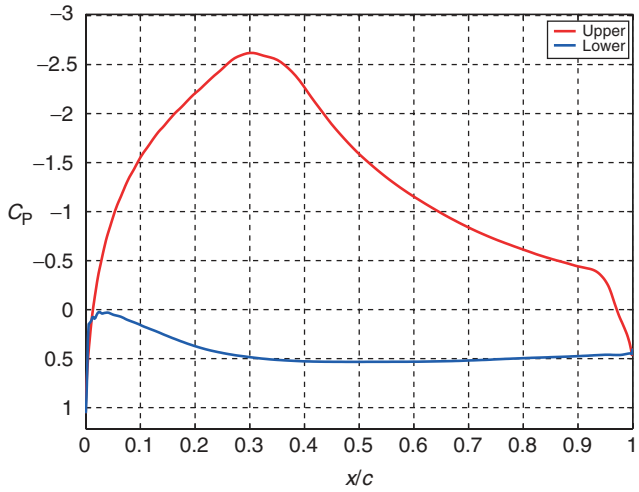

Figure 8. *C_P over the airfoil profile.*

thickness $t = 0.4\,\text{mm}$. The softer skin is chosen to promote axial deformations due to chordwise bending of the wing profile. Free-stream properties are assumed to be those at sea-level, with a Mach number of $M = 0.45$, and an angle of attack $\alpha = 2^\circ$. Such free-stream conditions produce the pressure distribution shown in Figure 7, where $p_\infty/\rho v_\infty^2 = 3.53$. The corresponding structural loads are depicted in Figure 10, while the resulting deformed configurations of airfoils of different core designs are presented in Figure 11. Specifically, Figure 11a corresponds to a core characterized by the ratio L/R, defining ligament length versus distance between centers of the nodes, equal to 0.60, while the core in Figure 11b is obtained for $L/R = 0.80$. The first core design features an upward deflection $\simeq 2.75\,\text{cm}$, while the second core is significantly stiffer, as the tip displacement under the same conditions is more than one order of magnitude lower ($\simeq 0.22\,\text{cm}$). Such a difference in compliance is obtained by only varying a single parameter, while maintaining material and geometric parameters constant. Such capabilities demonstrate the sensitivity of the considered design to

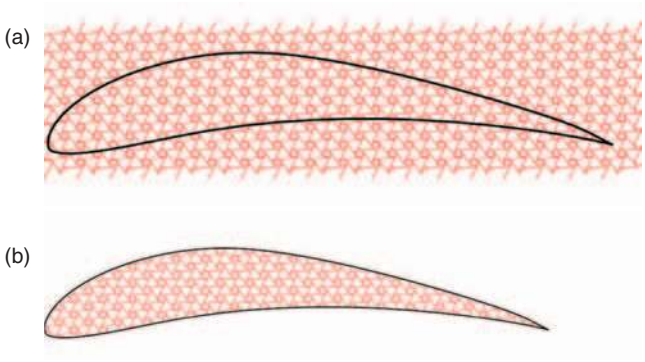

Figure 9. *Eppler airfoil superimposed to regular, periodic chiral layout (a), and resulting truss-core airfoil (b).*

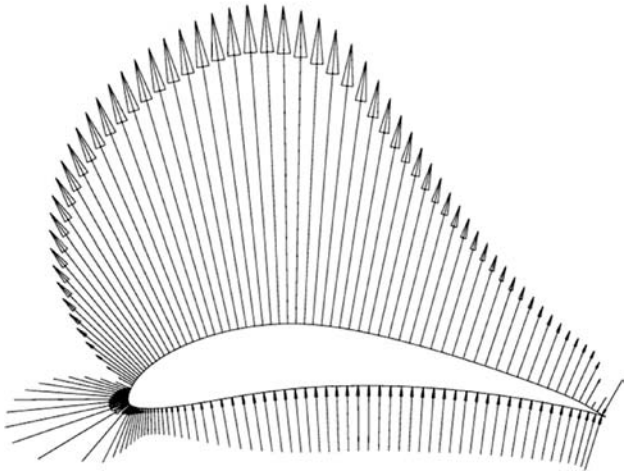

Figure 10. *Air loads corresponding to assigned flow conditions.*

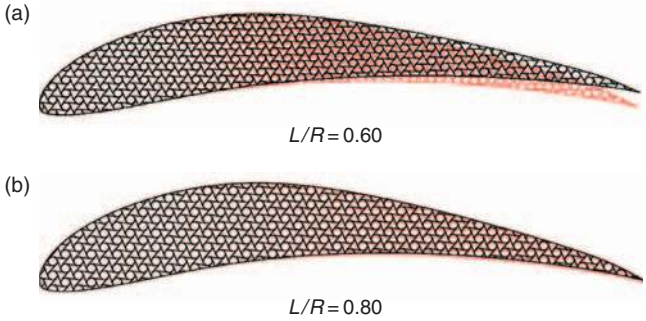

Figure 11. *Deformed configurations obtained with two core designs.*

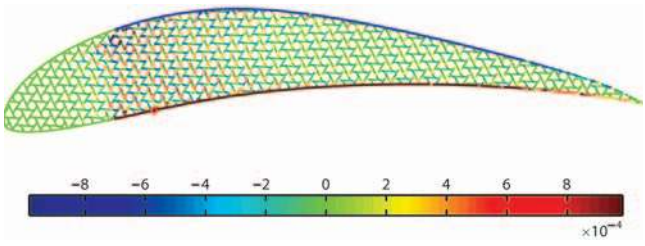

Figure 12. *Axial strain distribution corresponding to deformed configuration of Figure 11a.*

small changes in the core configuration, which may be optimized to achieve the desired compliance, or in general the required functionality. The optimization is potentially very easy to perform as a single variable, in this case L/R, defines the behavior of the structural assembly. These results suggest that ribs of the kind considered here may be manufactured to obtain different levels of compliance at different locations along the wing, for example. The manufacturing can be performed using same material and same basic geometry. The deflection in Figure 11a, for L/R=0.60, corresponds to the distribution of axial strain in the ligaments shown in Figure 12. It is interesting to observe how the maximum strain levels in the core are of the order of 1×10^{-3}, and therefore can be considered safely within the linear-elastic region of the constituent material.

Design Configuration 2

The information obtained from the analysis of the strain distribution is used to simplify the design of the considered truss-core structure. In the second design indeed, the chiral geometry only occupies a limited portion of the airfoil, which corresponds to the region of highest strain observed in the previous simulation (Figure 12). The chiral layout is modified to better fit the airfoil shape, as depicted in Figure 1b. This choice also facilitates the meshing process and simplifies future manufacturing of the assembly. The schematic of the process for the generation of this modified layout is shown in Figure 13. The core configuration is defined by assigning the parameters of the chiral topology (L/R) in the not-deformed configuration, and the number of cells along the longitudinal and transverse directions r, s. The resulting regular, periodic configuration is then mapped into the curved geometry of the airfoil through a simple change in coordinates. Examples of configurations featuring 2 and 5 chiral cells across the thickness of the airfoil are shown in Figure 14.

The performance of this second design is evaluated for the same free-stream conditions previously considered. The airfoil chord is now 0.7 m, while both the core and

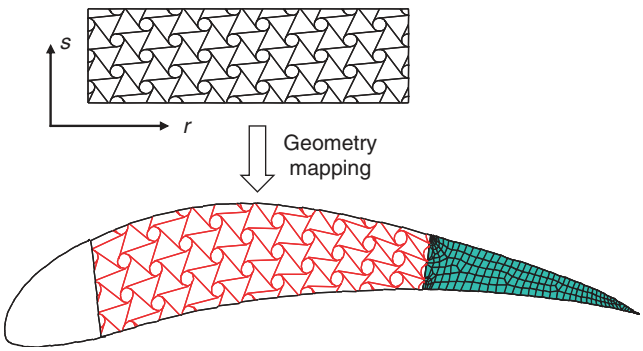

Figure 13. *Mapping of chiral layout in airfoil shape.*

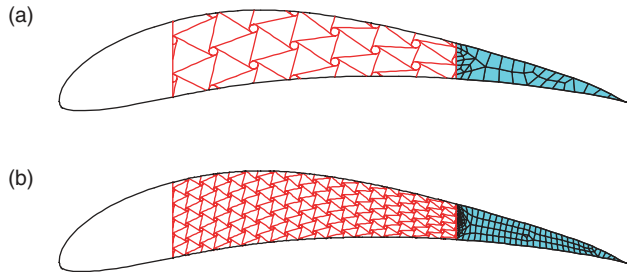

Figure 14. *Chiral-core airfoil with 2 (a) and 5 (b) unit cells across the thickness.*

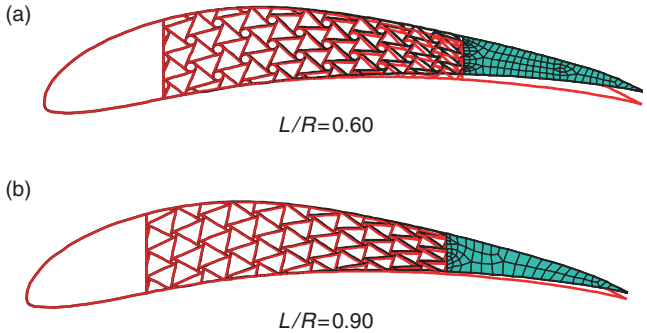

Figure 15. *Deformed configurations with 3 unit cells across the one thickness and two values of L/R ratio.*

outer skin have a wall thickness t equal to 0.76 mm. The choice of the chord length is driven by limitations imposed by manufacturing considerations for future implementations of the concept. The core and the top part of the skin are made of aluminum, while the lower section of the skin is modeled as a different material which may be made softer to facilitate the desired bending deformations. Deformed configurations for core with 3 cells across the thickness are compared in Figure 15, which confirms that the core design significantly affects the structure's compliance. The core with $L/R = 0.60$ undergoes a total tip deflection of $\sim$1.3 cm, while the one with $L/R = 0.90$ only deflects about 0.67 cm. Such different behaviors can be partially explained by considering the bending deformation of the ligaments in conjunction with the rotation of the nodes as the main contributor to the overall deflection of the structure (Prall and Lakes, 1996). Smaller L/R ratios correspond to nodes of larger diameter, which, through rotation of the ligaments, can generate larger bending moments at the ends of the ligaments. This is counteracted by the fact that as the node radius increases, the ligament's length decreases thus increasing their bending stiffness. A compromise may exist and optimal L/R ratios may require investigations in future developments. The main deformation mechanism may be understood from Figure 16, which shows details of the core corresponding

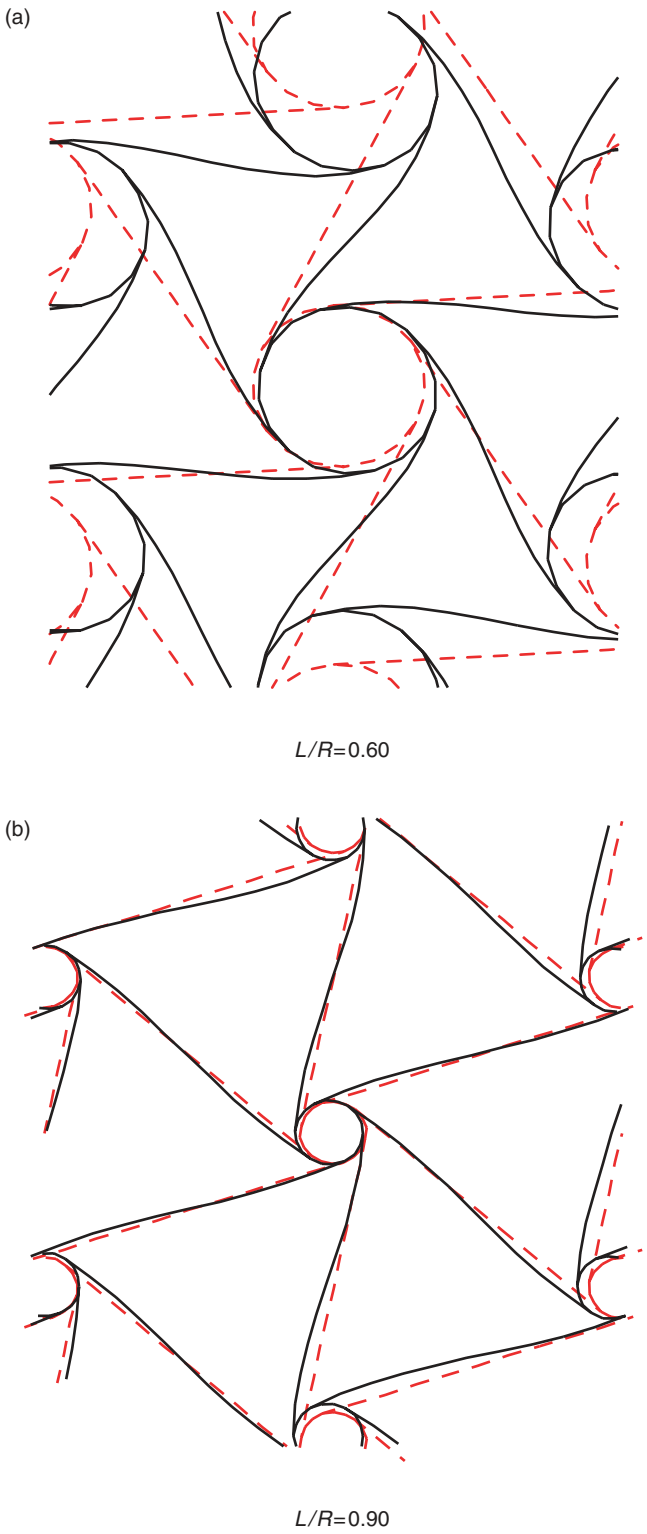

Figure 16. *Detail of core deformation for two values of the L/R ratio.*

to the deformed configurations shown in Figure 15. Figure 16 shows how larger nodes cause a noticeable bending in the ligaments as opposed to the case of small nodes.

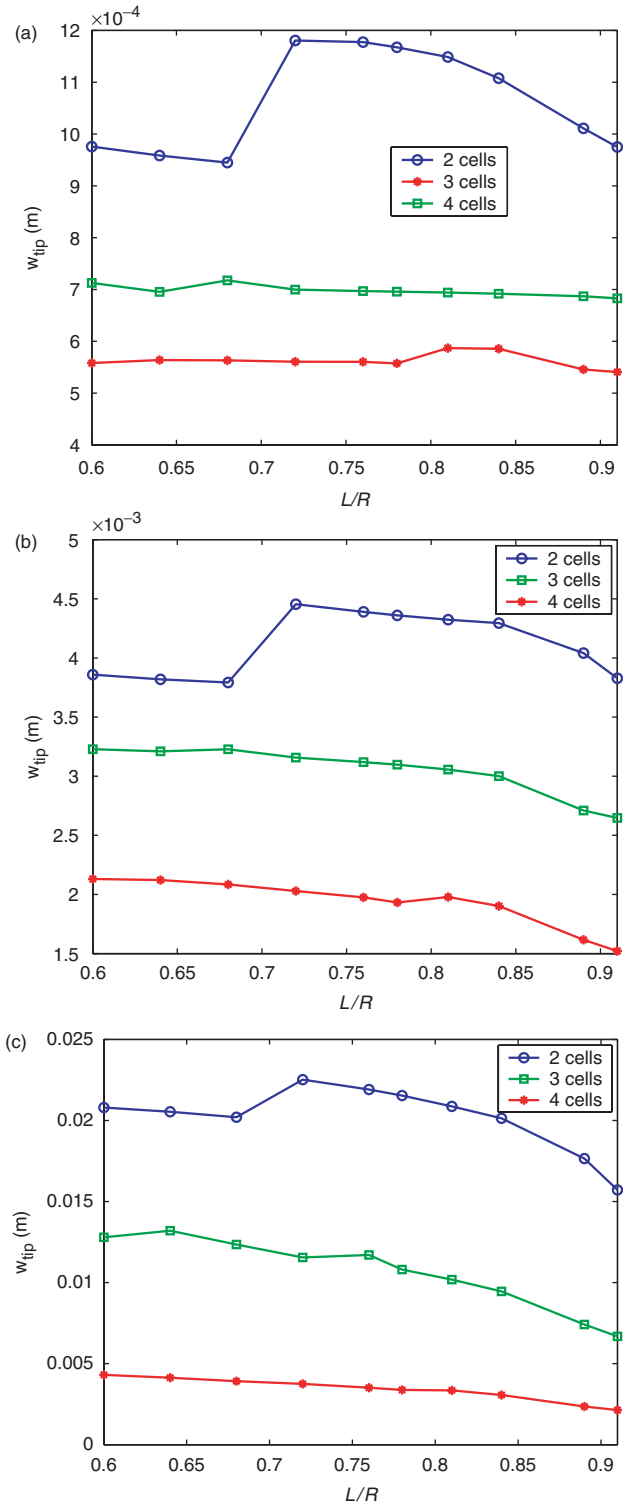

Figure 17. *Trailing edge tip displacement for various values of bottom skin Young's modulus: (a) $E_s = 7.1 \times 10^{10}$, (b) $E_s = 7.1 \times 10^{9}$, and (c) $E_s = 7.1 \times 10^{8}$.*

A summary of the performance of the considered airfoil is presented in Figure 17 where the displacement of the trailing edge for the considered flow conditions and various core configurations is plotted versus the L/R ratio. Results are presented for varying number of cells across the thickness of the airfoil, namely 2, 3, and 4, and for changing values of the Young's modulus of the lower skin. The plots confirm that large nodes as resulting from low numbers of cells through the thickness yield greater compliance. The variations with respect to L/R show a general trend as predicted by the previous analysis, but also indicates peculiar characteristics for $L/R \approx 0.70$ where a maximum in compliance is observed. The occurrence of such maximum values of displacement may result from the compromise between node radius, ligament length, and corresponding flexibility. Deformed configurations corresponding to the plots of Figure 17c for the design with 2 cells across the thickness are shown in Figure 18, which suggest how in spite of larger tip deflections for $L/R = 0.72$, the general deformed configurations of the airfoil appear very similar. The existence of optimal values of L/R to maximize compliance are currently under investigation, in conjunction with experimental validations of the findings presented in this article. Another parameter that clearly has great influence on the airfoil performance is the skin stiffness, as dictated by the Young's modulus of the constitutive material. As the results show, and as expected, the lower the skin's Young's modulus the higher the compliance. The lower limit considered in the investigations corresponds to values for which the skin undergoes significant displacements due to aerodynamic loads. Evidence of such deformations can be observed in Figure 18. It is interesting to note that the axial strain corresponding to these deformed configurations is still low and does not reach yield levels, and that all the configurations produce continuous deflections of the airfoil.

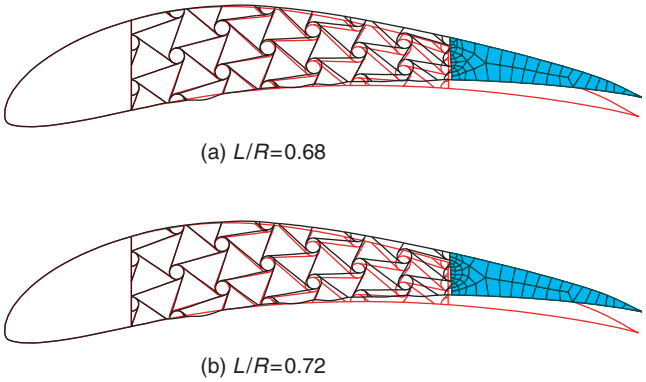

Figure 18. *Deformed configurations with 2 unit cells across the one thickness and two values of L/R ratio.*

CONCLUSIONS

This article presents a morphing concept where the core of an airfoil features a truss-like structure of chiral geometry. Such layout offers the ability to sustain large

deformations while undergoing relatively small strain. In addition, the compliance of the assembly can be significantly modified through the selection of a limited number of parameters which defines the basic chiral topology. A numerical model is developed to predict the airfoil deflection resulting from assigned flow conditions. The presented numerical results demonstrate the compliant characteristics of the considered configuration and its design flexibility, which could be employed for the optimization of the considered morphing concept. A prototype chiral-core airfoil is being manufactured and will be tested in the near future to validate the numerical predictions and to demonstrate the concepts illustrated in the article.

ACKNOWLEDGMENTS

This work is supported by the Army Research Office (ARO) project 45518-EG. The authors wish to thank the program manager and technical monitor, Dr Gary Anderson, for his support and technical inputs.

REFERENCES

Bae, J.S., Seigler, T.M., Inman, D.J. and Lee, I. 2004. "Aerodynamic and Aeroelastic Consideration of a Variablespan Morphing Wing," In: AIAA-2004-1726, 45th AIAA/ASME/ASCE/AHS/ASC Structures, Structural Dynamics and Materials Conference, Palm Springs, California, April 19–22.

Bornengo, D., Scarpa, F. and Remillat, C. June 2005. "Morphing Airfoil Concept with Chiral Core Structure," In: Proceedings of the I MECH E Part G, *Journal of Aerospace Engineering*, G3(8):185–192.

Bowman, J., Sanders, B. and Weisshaar, T. 2002. "Identification of Military Morphing Aircraft Missions and Morphing Technology Assessment," In: *Proceedings of SPIE Smart Materials and Structures*, 17 March, San Diego, CA, pp. 121–132.

Buter, A., Ehlert, U.C., Sachau, D. and Breitbach, E. 2000. "Adaptive Rotor Blade Concepts, Direct Twist and Camber Variation," In: AVT Symposium, Braunschweig.

Cadogan, D., Smith, T., Uhelsky, F. and MacCusick, M. 2004. "Morphing Airfoil Wing Development for Compact Package Unmanned Aerial Vehicles," In: AIAA-2004-1807, 45th AIAA/ASME/ASCE/AHS/ASC Structures, Structural Dynamics and Materials Conference, Palm Springs, CA, 19–22 April.

Campanile, L.F. and Sachau, D. 2000. "The Belt-Rib Concept: A Structronic Approach to Variable Camber," *Journal of Intelligent Materials Systems and Structures*, 11(3):215–224.

Cook, R.D., Malkus, D.S., Plesha, M.E. and Witt, R.J. 2001. *Concepts and Applications of Finite Element Analysis*, 4th edn, Vol. II, Wiley, New York, NY.

Kudva, J.N. 2004. "Overview of the DARPA Smart Wing Project," *Journal of Intelligent Materials Systems and Structures*, 15(4): 261–267.

McGowan, A.R., Cox, D.E., Lazos, B.S., Waszak, M.R., Raney, D.L., Siochi, E.J. and Pao, P.S. 2003. "Biologically Inspired Technologies in NASA's Morphing Project," In: *Proceedings of SPIE Smart Structures and Materials*, 15–20 March, San Diego, CA, pp. 1–13.

Mohammadi, B. 1994. "Fluid Dynamics Computation with NSC2KE," INRIA Report 0164.

Monner, H.P., Sachau, D. and Breitbach, E. 1999. "Design Aspects of the Elastic Trailing Edge for an Adaptive Wing," pp. 14/1–14/8, Research and Technology Agency, Ottawa, Canada, 18–21 October.

Prall, D. and Lakes, R.S. 1996. "Properties of a Chiral Honeycomb with Poisson's ratio of -1," *International Journal of Mechanical Sciences*, 39(3):305–314.

Spadoni, A., Ruzzene, M. and Scarpa, F. 2005. "Dynamic Response of Chiral Truss-Core Assemblies," *Journal of Intelligent Materials Systems and Structures*, 17(11):941–952.

Trenker, M. 2003. "Design of Adaptive Airfoils with Dynamic Transonic Flow Control," *Journal of Aircraft*, 40(4): 734–740.